Charge transport in purple membrane monolayers: A sequential tunneling approach

E. Alfinito,* J.-F. Millithaler,† and L. Reggiani‡

Dipartimento di Ingegneria dell'Innovazione, Università del Salento, via Monteroni, I-73100 Lecce, Italy, EU and Consorzio Nazionale Italiano di Struttura della Materia,via della Vasca Navale, 84, I-00146, Roma, Italy, EU

(Received 10 January 2011; published 21 April 2011)

Current-voltage (I-V) characteristics in proteins are sensitive to conformational changes induced by an external stimulus (photons, chemical, etc.). This sensitivity can be used in medical and industrial applications as well as shedding new light on the microscopic structure of biological materials. Here, we show that a sequential tunneling model of carrier transfer between neighboring amino acids in a single protein is the basic mechanism responsible for the electrical properties measured over a wide range of applied potentials. We also show that such a strict correlation between the protein structure and the electrical response can lead to a new generation of nanobiosensors that mimic the sensorial activity of living species. To demonstrate the potential usefulness of protein electrical properties, we provide a microscopic interpretation of recent I-V experiments carried out in bacteriorhodopsin at a nanoscale length.

DOI: 10.1103/PhysRevE.83.042902 PACS number(s): 87.14.ef, 82.39.Jn, 87.15.hp

The nature of electron transport (ET) in biological material is of outstanding interest, both for pure speculative reasons and for applications. As a matter of fact, organic- and biological-based devices are the new frontier of technology, due to their potential low cost, low size, high specificity, etc. [1,2]. Usually, biological materials are not easy to investigate, because a standard way of preparation is still not available [2]. Nevertheless, there are some relevant exceptions, like monolayers of purple membrane (PM), a part of the cell membrane of the halophile *Halobacterium salinarum*, which is easy to prepare and suitable for direct measurements. PM is made of a single type of protein, the light receptor bacteriorhodopsin (bR), organized in trimers and stabilized by lipids [3]. The entire structure appears as a two-dimensional (2D) hexagonal crystal lattice. The natural role of bR is to use sunlight for pumping protons outside the cell and in doing so, it changes its tertiary structure (conformational change).

Recently, current-voltage (I-V) characteristics of purple membrane were analyzed under different experimental conditions [4–6], giving clear evidence of super-Ohmic and illumination-dependent responses [4]. These measurements are of paramount importance for understanding the mechanism of ET, and also for protein activation; furthermore, they may aid the development of a new generation of organic-based devices [7]. The seminal experiment [4] was carried out on metal-insulator-metal (MIM) junctions of millimetric diameter, where the insulator was a 5 nm monolayer of PM. The measurements covered a small range of bias (0–1 V), because of the high value of the current response (nA level). The response was found to be slightly super-Ohmic and grows overall by a factor of 2 when the sample is irradiated by a green light. These results suggest that in this protein, as in some organic polymers [8], ET is ruled by tunneling mechanisms. Furthermore, the large thickness of PM (5 nm) strongly suggests the possibility of multiple carrier jumps across the protein (*sequential* tunneling) [4,6].

In a later experiment [5], the I-V characterization was performed at the *nanometric* scale, with the technique of conductive atomic force microscopy (c-AFM). Accordingly, one of the contacts was the tip of the c-AFM (with nominal radius 100–200 nm). With respect to the first measurement, in the common bias range, the current response is lower by about four orders of magnitude; thus the sample is able to sustain higher voltages, up to about 5–10 V. Measurements were performed without any extra light irradiation and with different tip indentations from about 4.6 down to 1.2 nm. At voltages above about 2 V, the presence of a crossover between the direct tunneling regime and the injection or Fowler-Nordheim (FN) tunneling regime was evidenced.

At present, a microscopic interpretation of the above experiments is still in its infancy and, apart from some attempts [5,9], a unifying approach able to explain the main features and, possibly, to be predictive for analogous physical systems is lacking. This paper aims to fill this lack of knowledge by implementing an ET model hereafter called the impedance network protein analog (INPA). The INPA uses a microscopic description of the protein tertiary structure that takes the amino acids as single centers of interaction, responsible for charge transfer. Finally, charge transport through a single protein is due to the simultaneous activation of multiple pathways in an *impedance network* as in the tunneling pathway method developed by Onuchic and co-workers [10]. The network approach has also strong analogies with a percolative process [11] and, thus, the solution of the transport problem is through a stochastic method. With respect to existing approaches [12,13], the INPA has some advantages: (i) the tertiary structure of the protein is directly correlated to the macroscopic observables; (ii) the different electrical responses in the presence or absence of a green light are reproduced; (iii) the interpretations of different data [4,5] are reconciled; and (iv) it can be applied to other proteins whose tertiary structure is known.

In brief, the structure of the INPA is as follows. The protein structure is coarse-grained and described by means of the C_α positions, as obtained by protein database (PDB) or homology modeling [9]. Each C_α position is taken as corresponding to a node in a graph whose links describe the electrical

*Corresponding author: eleonora.alfinito@unisalento.it
†jf.millithaler@unile.it
‡lino.reggiani@unisalento.it

interactions between amino acids. The degree of proximity for each node is assigned by a cutoff interaction radius, say R_C. In the present analysis, we choose $R_C = 6$ Å , a value that optimizes the native- to activated-state resolution [9]. Each link is associated with an impedance (a simple resistance in this case) whose value depends on the distance between amino acids. In particular: $r_{i,j} = \rho\, l_{i,j}/\mathcal{A}_{i,j}$, where ρ indicates the resistivity, here taken to be same for all links; ρ, in general, depends on the voltage as detailed below; the subscripts i, j refer to the amino acids between which the link is stretched; $l_{i,j}$ is the distance between the labeled amino acids taken as pointlike centers; and $\mathcal{A}_{i,j}$ is the cross-sectional area shared by the labeled amino acids: $\mathcal{A}_{i,j} = \pi(\mathrm{R}_C^2 - l_{i,j}^2/4)$. The graph is, thus, mapped onto an impedance network.

To take into account the superlinear response, ρ is chosen to depend on the voltage drop as

$$\rho(V) = \begin{cases} \rho_{\max}, & eV \leqslant \Phi, \\ \rho_{\max}\left(\frac{\Phi}{eV}\right) + \rho_{\min}\left(1 - \frac{\Phi}{eV}\right), & eV \geqslant \Phi, \end{cases} \quad (1)$$

where $\rho_{\max}$ is the resistivity value that should be used to fit the I-V characteristic at the lowest voltages, $\rho_{\min} \ll \rho_{\max}$ plays the role of an extremely low series resistance, limiting the current at the highest voltages, and Φ is the threshold energy separating the two tunneling regimes (a kind of effective height of a tunneling barrier). Since ET is here interpreted in terms of sequential tunneling between neighboring amino acids, the above interpolation formula reflects different voltage dependence in the prefactors of the current expression [14]: $I \sim V$ in the direct tunneling regime, and $I \sim V^2$ in the FN tunneling regime.

For the transmission probability of the tunneling mechanism we take the expression given by Refs [5,15]:

$$\mathcal{P}_{i,j}^{D} = \exp\left[-\frac{2l_{i,j}}{\hbar}\sqrt{2m\left(\Phi - \frac{1}{2}eV_{i,j}\right)}\right], \quad eV_{i,j} \leqslant \Phi, \quad (2)$$

$$\mathcal{P}_{i,j}^{\mathrm{FN}} = \exp\left[-\left(\frac{2l_{i,j}\sqrt{2m}}{\hbar}\right)\frac{\Phi}{eV_{i,j}}\sqrt{\frac{\Phi}{2}}\right], \quad eV_{i,j} \geqslant \Phi; \quad (3)$$

where $V_{i,j}$ is the local potential drop between two amino acids, i, j, and m is the electron effective mass, here taken to be the same as the bare value.

Figure 1 reports the shape of the tunneling transmission probability that includes both the direct and injection regimes (continuous curve) together with that corresponding to direct tunneling only (dashed curve).

In the solution of the resistor network, the tunneling mechanism is accounted for by the following procedure. First, the network is electrically solved by using the value $\rho_{\max}$ for all the elemental resistances. Second, by using a Monte Carlo acceptance-rejection procedure, each $\rho_{\max}$ is stochastically replaced by $\rho_{\min}$ using the probability in Eqs. (2) and (3) according to the local potential drops calculated in the first step. In the high-voltage region ($eV_{i,j} > \Phi$), if the stochastic procedure gives a rejection, then $\rho_{\max}$ is replaced by $\rho(V_{i,j})$ of Eq. (1). The network is then electrically updated with the new distributed values of $\rho(V_{i,j})$. Third, the electrical update is iterated (typically 10^6–10^8 iterations depending on the value of the applied voltage) by repeating the second step until the value of the network-associated current converges within an uncertainty less than a few percent.

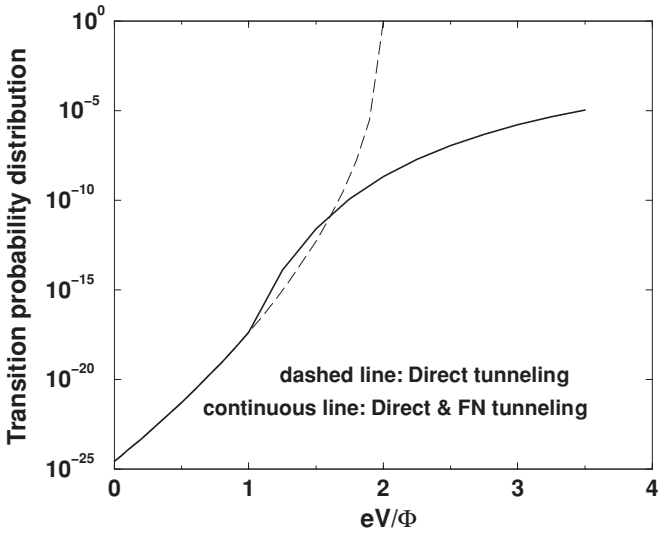

FIG. 1. Transmission probability for the two tunneling regimes

To model bacteriorhodopsin in its native state (in the dark) [9] we used the PDB entry 2NTU. The network was then studied with two different contact configurations: pointlike contacts (in line with previous work) and extended contacts. In the first configuration, the network was connected to the external bias by means of perfectly conductive contacts, the input on the first amino acid, and the output on the last amino acid of the primary structure. In the second configuration, the input simulates the extended tip of the AFM device. Accordingly, all nodes with a z coordinate (in the direction of the tip penetration) larger than that of the first amino acid assume the same potential value. The output, pointlike, remains on the last amino acid.

The values of $\rho_{\max}$, $\rho_{\min}$, and Φ were obtained by fitting the experiments of [5] corresponding to an electrode distance of $L = 4.6$ nm. For this distance, the measurements are associated with a current crossing a single layer of proteins. Actually, we found $\rho_{\max} = 4 \times 10^{13}\Omega$ Å , $\rho_{\min} = 4 \times 10^{5}\Omega$ Å , and $\Phi = 219$ meV. The large difference between the $\rho_{\max}$ and the $\rho_{\min}$ values is dictated by the six orders of magnitude spanned by the current values. The values of $\rho_{\max}$ and $\rho_{\min}$ correspond to the macroscopic resistance given by the V/I ratio of the experiment. In that case, the current measured at 1 V in Ref. [4] yields the number of trimers to be equal to about $N = 10^9$ for a sample area of 2×10^{11} nm^2, thus giving a resistivity of about 10^{20} Ω Å for a trimer [9]. By assuming, in the present case, the same trimer resistivity, we estimate that the number of trimers involved in the measured current is about $N = 10^6$, thus leading to a crossing area of about 10^7 nm^2. However, within a MIM electrical analog, in [5] the effective area deduced by the fit was found to be $0.1\times$ nm^2, about eight orders of magnitude smaller than estimated above. This dramatic difference is mainly attributed to the MIM electrical analog used in Ref. [5] that contrasts with the sequential tunneling model used here.

Figure 2 compares the numerical and experimental data for the extended contact model and the pointlike contact model

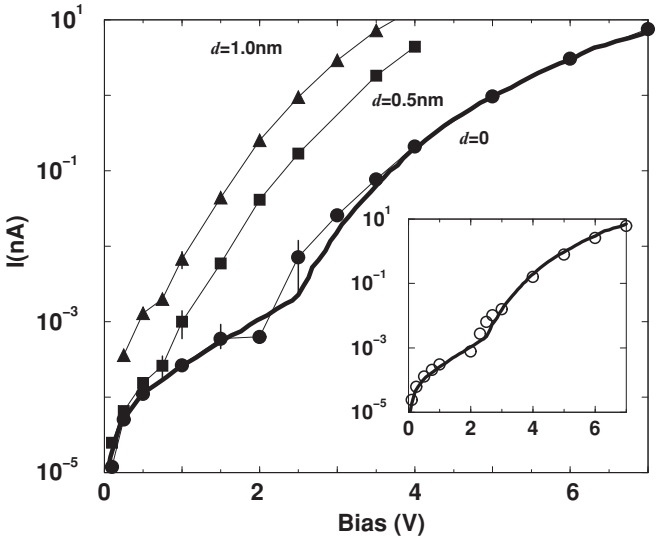

FIG. 2. I-V characteristics obtained by simulations with extended contacts at the different indentations. The symbols and the thin dashed curves refer to calculations. The thick continuous line is experimental data in the absence of indentation ($d = 0$) when the electrode distance is 4.6 nm [5]. The symbols in the inset show the theoretical fit for $d = 0$ performed with pointlike contacts (see text).

at $L = 4.6$ nm (in the inset). In both the cases, the agreement is within the experimental and numerical uncertainties, and thus considered to be satisfactory. The threshold energy $\Phi = 219$ meV is taken to be independent of the contact choice. On the other hand, when going from the pointlike to the extended contact configuration, the fitting values of $\rho_{\max}$ increase from 4×10^{13} to 8×10^{13} Ω Å and also those for $\rho_{\min}$ increase from 4×10^{5} to 4×10^{6} Ω Å.

The position of the extended contact is then changed in order to reproduce the experimental results obtained for different values of the indentation of the tip. At increasing depths of the extended contact, the net effect is a reduced number of amino acids involved in electrical transport. As a consequence, higher currents and a shift to lower potential values for the crossover between the direct and the FN regime are expected. Numerical calculations, as shown in Fig. 2, confirm these expectations. In particular, the flat contact that simulates the tip indentation was placed at depths of 0.50 and 1.0 nm from the top of the protein. For these depths, the experimental data at increasing tip indentations exhibit a quantitative agreement with the modeling in the region of high voltages where FN tunneling prevails. Even if the experimental indentation of the tip is greater by about a factor of 3 with respect to that of the simulations, we consider the agreement between theory and experiments to be satisfactory in view of the simplifications needed to convert the single-protein calculation into the macroscopic value measured. However, at low voltages the results of the simulations underestimate by up to an order of magnitude the values of the experiments. The disagreement at low voltages is here overcome by assuming the existence of a leakage contribution, probably associated with the complexity of the contact regions, constituted by trimers and lipids, with respect to the model used [16]. Accordingly, the single resistance associated with each link is replaced by two parallel resistances, one pertaining to the protein and the other to a more realistic modeling of the contact regions.

Figure 3 reports the currents for different indentations when an Ohmic leakage current is added to the values shown in Fig. 2. The best fit is obtained by taking for the leakage resistance the values 8.4×10^{12}, 0.11×10^{12}, and 0.036×10^{12} Ω, respectively for L values of 4.6, 2.8, and 1.2 nm. The leakage resistance at $L = 4.6$ nm is taken to be equal to the protein resistance value at low bias. The decrease of the leakage resistance at increasing indentation can be related to geometrical effects associated with the decreasing

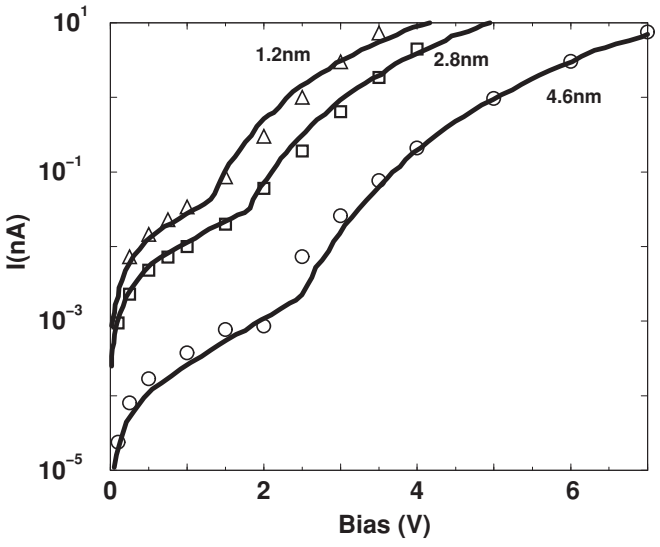

FIG. 3. I-V characteristics obtained by simulations with extended contacts at the different indentations including a leakage current. The thick continuous lines show experimental data [5] and the symbols numerical simulations.

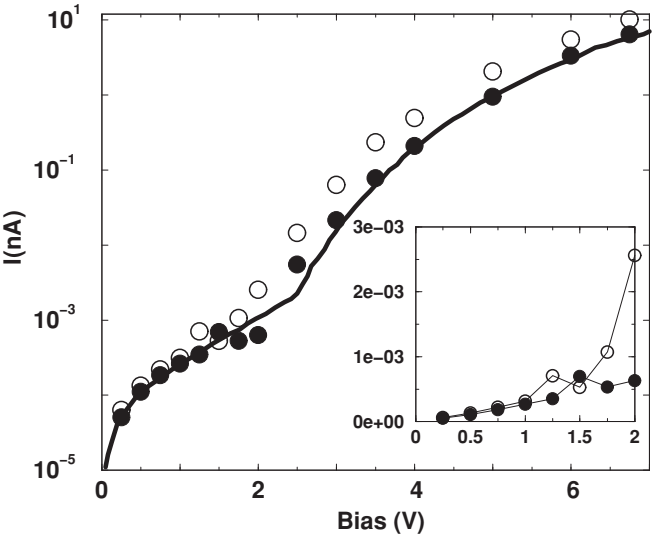

FIG. 4. I-V characteristics for the native and activated states of bR performed with pointlike contacts. Filled and unfilled symbols refer to native and activated states, respectively. The thick curve was for experiments with an electrode distance $L = 4.6$ nm [5]. In the inset the current is rescaled to reproduce the measured value of the native state at 1 V given in Ref. [4].

of the interelectrode distance and the increasing surface of the tip contact when penetrating the protein. Interestingly enough, the microscopic interpretation is obtained with a length-independent electron effective mass, contrary to the case of Ref. [5], where to fit experiments, the carrier effective mass should increase by over one order of magnitude when increasing the indentation. [We notice that a larger (smaller) value of the effective mass would produce a shift to a lower (higher) value of the transmission probability, which can be compensated by a corresponding change in the value of the energy threshold without significant modifications of the microscopic interpretation.] Most importantly, the value of the energy threshold is reduced, by about a factor of 10, when compared with the values of the barrier height found in Ref. [5]. Both these features are a consequence of the sequential tunneling mechanism assumed here, and which replaces the single-tunneling mechanisms of the MIM model previously used [5].

As anticipated above, the INPA is able to interpret the behavior of the *I-V* characteristics carried out with an *electrode-bilayer-electrode* structure and when the protein is illuminated or not by green light [4]. To this purpose, the model is applied to the PDB entry 2NTW (describing the activated state of bR) [9] and the data, calculated with the same parameters used for calculating the *I-V* characteristic of the native state, for the extended contact configuration. Figure 4 reports the simulated data calculated for both the native and activated states. The trend evidenced by experiments is here reproduced without introducing arbitrary parameters. We notice that the present results are compatible with those reported by some of the authors in Ref. [9]. Here, the higher value of Φ used to fit the data of Ref. [5] leads to some minor differences in the current responses of the native and activated states, which should be justified by the complexity of the physical system investigated.

In conclusion, we propose a sequential tunneling mechanism for charge transport in bacteriorhodopsin. The model permits a consistent interpretation of a set of experiments carried out in a wide range of applied electrical potentials and in the presence or not of an external green light. The tertiary structure of the protein is used as direct data input and enables one to relate quantitatively conformational change and the sensing action of the protein. Finally, data obtained under very stressing conditions, like the penetration of an AFM tip into the protein membrane, can be finely reproduced. The qualitative and quantitative agreements between the numerical results and experiments means that the INPA, implemented here for a sequential tunneling mechanism, is a physically plausible model to investigate electrical properties in other proteins pertaining to the transmembrane family.

This research is supported by the European Commission under the Bioelectronic Olfactory Neuron Device (BOND) project within the Grant Agreement No. 228685-2.

[1] W. Göpel, Sens. Act. B **65**, 70 (2000); A. Dodabalapur, L. Torsi, and H. E. Katz, Science **268**, 270 (1995) ; A. Corcelli, S. Lobasso, P. Lopalco, M. Dibattista, R. Araneda, Z. Peterlin, and S. Firestein, J. Haz. Mater. **175**, 1096 (2010).

[2] Y. Hou *et al*., Biosens. Bioelectron. **22**, 1550 (2007).

[3] A. Corcelli, M. Colella, G. Mascolo, F. P. Fanizzi, and M. Kates, Biochemistry **39**, 3318 (2000).

[4] Y. D. Jin, N. Friedman, M. Sheves, T. He, and D. Cahen, Proc. Natl. Acad. Sci. USA **103**, 8601 (2006); Y. D. Jin, N. Friedman, M. Sheves, and D. Cahen, Adv. Funct. Mater. **17**, 1417 (2007).

[5] I. Casuso, L. Fumagalli, J. Samitier, E. Padrós, L. Reggiani, V. Akimov, and G. Gomila, Nanotechnology **18**, 465503 (2007).

[6] I. Ron, L. Sepunaru, S. Itzhakov, T. Belenkova, N. Friedman, I. Pecht, M. Sheves, and D. Cahen, J. Am. Chem. Soc. **132**, 4131 (2010).

[7] A. M. Kannan, V. Renugopalakrishnan, S. Filipek, P. Li, G. F. Audette, and L. Munukutla, J. Nanosci. Nanotech. **9**, 1665 (2009).

[8] I. Zvyagin, in *Charge Transport in Disordered Materials*, edited by S. Bartlett (J. Wiley & Sons, Chichester, 2008).

[9] E. Alfinito and L. Reggiani, Europhys. Lett. **85**, 86002 (2009), and references therein.

[10] D. N. Beratan, J. N. Onuchic, J. N. Betts, B. E. Bowler, and H. B. Gray, J. Am. Chem. Soc. **112**, 7915 (1990), and references therein.

[11] C. Pennetta, Gy. Trefan, and L. Reggiani, Phys. Rev. Lett. **85**, 5238 (2000).

[12] D. M. Adams *et al*., J. Phys. Chem. B **107**, 6668 (2003).

[13] A. Nitzan, e-print arXiv:cond-mat/0102300.

[14] W. Wang, T. Lee, and M. A. Reed, Rep. Prog. Phys. **68**, 523 (2005); W. Wang, T. Lee, I. Kretzschmar, and M. A. Reed, Nano Lett. **4**, 643 (2004); W. Wang, T. Lee, and M. A. Reed, Phys. Rev. B **68**, 035416 (2003).

[15] J. G. Simmons, J. Appl. Phys. **34**, 1793 (1963).

[16] T. Hianik, in *Bioelectrochemistry: Fundamentals, Experimental Techniques and Applications*, edited by P. N. Bartlett (J. Wiley & Sons, Chichester, 2008).